



Article

Reduced Graphene Oxide: Effect of Reduction on Electrical Conductivity

Sanjeev Rao ^{1,2,*} , Jahnavee Upadhyay ¹, Kyriaki Polychronopoulou ³, Rehan Umer ² and Raj Das ¹

¹ Centre for Advanced Composite Materials, Department of Mechanical Engineering, The University of Auckland, Auckland Mail Centre, Auckland 1142, New Zealand; s.rao@auckland.ac.nz (J.U.); r.das@auckland.ac.nz (R.D.)

² Areospace Research and Innovation Centre (ARIC), Khalifa University of Science, Technology and Research, P.O. Box, Abu Dhabi 127788, UAE; rehan.umer@kustar.ac.ae

³ Department of Mechanical Engineering, Khalifa University of Science, Technology and Research, P.O. Box, Abu Dhabi 127788, UAE; kyriaki.polychrono@kustar.ac.ae

* Correspondence: sanjeev.rao@kustar.ac.ae; Tel.: +971-2-5018509

Received: 5 March 2018; Accepted: 4 April 2018; Published: 9 April 2018



Abstract: In this study, the effect of reduction on the electrical conductivity of Graphene Oxide (GO) is investigated. The aim of this fabrication was to render electromagnetic interference (EMI) shielding to thin polymer films using GO as fillers. The electrical conductivity was determined using the four-probe method and shielding effectiveness was theoretically determined using the experimentally obtained conductivity values. The initial oxidation of graphite was performed using Hummers' method and the oxidized GO was dispersed in water for further exfoliation by ultrasonication. Thin films of sonicated GO dispersions were solution casted and dried in a convection oven at 50 °C overnight. The dried films were treated with 48% hydrobromic acid (HBr), 95% hydrochloric acid (HCl) or 66% hydroiodic acid (HI) for 2 h, 24 h or 48 h. A partial factorial design of experiments based on Taguchi method was used to identify the best reducing agent to obtain maximum electrical conductivity in the partially reduced GO films. The experimental analysis indicates that the electrical resistivity of GO is highly dependent on the type of acid treatment and the samples treated with HI acid exhibited lowest resistivity of ~0.003 Ω·cm. The drop in resistivity value after chemical reduction was of the order of 10,000 times, and range obtained in this work is among the lowest reported so far. The theoretical EMI shielding of the reduced GO film provided a shielding effectiveness of 5.06 dB at 12 GHz.

Keywords: graphene oxide; FTIR; EMI; Taguchi; electrical conductivity

1. Introduction

With recent advances in material science, nanocomposites with exfoliated nanofillers have attracted considerable attention due to the superior mechanical and functional properties offered by the fillers at relatively lower filler loadings. Exfoliated graphene oxide (GO) as filler in particular has received considerable attention because of its mechanical and functional properties that are comparable to those of single-layered graphene with the ease of synthesis compared to that of graphene [1–3].

Considering the proximity of GO to graphene, polymer-GO nanocomposites have potential applications in memory devices and energy storage cells where the low conductivity of GO can help in creating a barrier for inter-lamellar electron-hole re-combinations. Other applications can be in field effect transistors, solar cells, energy storage devices, etc. Additionally, they appear to improve the resistance to gas permeability, suggesting potential for applications in food and beverage, packaging,

and filtration applications [1,4–7]. An interesting example where the conductive properties of the polymer-GO composites can be utilized is in ElectroMagnetic wave Interference (EMI) shielding and are currently emerging is a new class of materials for broad-band electromagnetic absorption [1,3,7–16].

GO is inherently non-conductive because of the absence of percolating pathways between sp^2 carbon clusters which is indeed a carrier transport mechanism in the graphene. A single sheet of graphene oxide consists of a hexagonal ring-based carbon network having both sp^2 -hybridised and sp^3 -hybridised carbon atoms, bearing hydroxyl and epoxide functional groups on either side of the sheet, whereas the sheet edges are mostly occupied by carboxyl and carbonyl groups [17–21], meaning that the functional groups attached to the plane influence its conductivity, while functional groups attached to the edge may not. GO as a whole on the contrary has large chemical functional groups attached to the carbon plane with several structural defects within the plane, both of which may severely decrease the electrical conductivity. However, it can be restored by varying their synthesis and processing, as they are non-stoichiometric in nature. A common approach is to attach polymers or polymerization initiators on to the GO platelets and reduce the oxidized surface [4]. This reduction process must aim at eliminating only the epoxy and hydroxyl groups on the plane, while retaining other groups, such as carboxyl, carbonyl, and ester groups at the edges.

There are different routes to synthesize GO for conductivity [22], out of which thermal and chemical routes are widely accepted to restore electrical conductivity. In the thermal reduction method, GO is exposed to temperature ramp rates greater than 2000 °C/min up to about 1050 °C, in effect splitting the graphite oxide into individual sheets through evolution of CO₂. The thermal shock decomposes the oxygen-containing groups attached to the carbon plane, and the escape of the resultant gases exfoliate the stacked graphene layers [5,9,11,23]. However, this process is suitable for bulk production, the yield is usually small, and the quality is poor with wrinkling and severe lattice defects. In the chemical route, GO is reduced using chemical reagents based on their chemical reactions with GO. Hydrazine is universally accepted as a good chemical reagent to reduce GO [2,17,24,25]. The reduction by hydrazine and its derivatives, such as hydrazine hydrate and dimethylhydrazine [12], is as simple as adding liquid reagents to aqueous dispersion of GO and drying it, wherein the reagents increase the hydrophobicity that results in agglomerated graphene-based nanosheets that may be electrically conductive. One drawback with this process is that the hydrazine agents usually tend leave C-N groups behind, in the form of hydrazones, amines, aziridines, etc., which may have detrimental effect on the electronic structure and properties of reduced GO [26,27]. However, by finely tuning the reduction parameters, it is possible to get rid of the C-N groups and indeed obtain electrically conductive GO. Therefore, in view of tuning the process parameters to achieve electrical conductivity, a systematic study on the effect of varying the process parameters on the electrical conductivity of the reduced GO discussed in this work.

For EMI shielding, conducting fillers in the form of nanocomposites are highly suitable due to ease of processing at relatively low costs with the benefit of various mechanical and functional properties of polymers. Polymer nanocomposites with carbon-based fillers have been extensively investigated in various works [23–27] with results showing their performance to be dependent on the type of matrix and filler [28,29], structural morphology and dispersion [26,27], processing method, matrix-filler interaction, etc. The EMI shielding effectiveness (EMI SE) of composite materials depends upon intrinsic conductivity of filler, its aspect ratio [30] and conductivity of the composite [31–34]. Therefore, primarily, EMI SE is a function of conductivity, but as the filler loading increases, the shielding will depend on the thickness of the specimen too, due to increased layering because of higher loading [30,35]. However, beyond percolation thresholds, the EMI shielding effectiveness also rises rapidly with the increase in electrical conductivity. However, the primary mechanism in such case is reflection due to interaction of incident radiation with the free electrons on the shield surface while absorption is the secondary mechanism. Therefore, the EMI SE can be tailored by varying the filler concentrations and their dispersion throughout the media. However, the medium of shielding effectiveness (absorption or reflection) may indeed vary accordingly.

In this study, a relatively novel chemical reduction method that uses hydrohalic acids for removal of oxygen-containing groups from GO, has been developed to tune the electrical conductivity of GO. Factorial design of experiments based on the Taguchi method was used to identify the key processing parameters and their synergistic effects, affecting the electrical property of the GO films. The post-reduction characterization of GO was performed using X-ray diffractometry, Fourier transfer infrared imaging and scanning electron microscopy.

2. Materials and Methods

Graphite flakes obtained from Sigma-Aldrich (Auckland, New Zealand) were powdered to particle size of 30 μm . 95–97% Sulfuric Acid (H_2SO_4) from Merck Group (Darmstadt, Germany) Potassium Permanganate (KMnO_4) from Ajax Chemicals, Australia, Sodium Nitrate NaNO_3 , 30% Hydrogen Peroxide (H_2O_2), 95% Hydrochloric acid (HCl), 48% Hydrobromic Acid (HBr) and 66% Hydroiodic acid (HI) from Ajax Finechem Inc. (Auckland, New Zealand) were used as-received. *N,N*-dimethylformamide (DMF, Anhydrous, 99.8%) and tetrahydrofuran (THF) were bought from Sigma-Aldrich and ECP Ltd. (Romil, Cambridge, UK), respectively, and the polymer matrix PMMA was bought from Chi Mei Corporation (Tainan, Taiwan).

Wide angle X-ray scattering (WAXS) technique was used to evaluate the crystallinity and inter-layer distance between adjacent layers of the multi-layered material. Fourier transfer infrared spectroscopy, FT-IR (Nicolet 8700, ATR-FTIR, Waltham, Massachusetts, USA), was used to confirm the presence/absence of oxygen-containing groups in GO after oxidization of graphite and partial reduction of GO, respectively. Scanning electron microscope, SEM (Philips XL30S FEG with Gatan Alto Cryo-trans System, Auckland, New Zealand), was used to visualize the GO sheets and nanofibers after platinum sputtering. The four-probe method developed in-house was used to measure the electrical conductivity of the GO sheets.

2.1. Graphene Oxide

Graphene oxide was synthesized using modified Hummers' method [29] and the details of the method can be found in the reference as listed, and pictures at various stages of chemical processing is shown in Figure 1. To achieve exfoliation, the GO obtained from the above process was dispersed in water and subjected ultrasonication. Thin films of sonicated GO dispersions were prepared by casting the mixture on petri dishes followed by drying in the oven at 50 $^{\circ}\text{C}$, overnight.

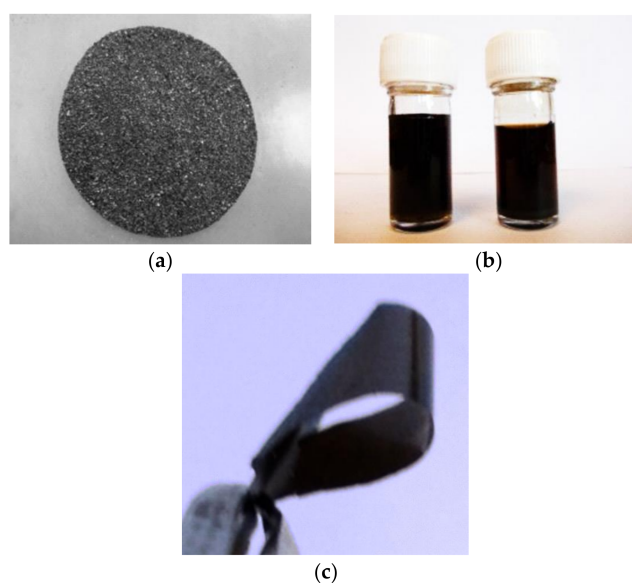


Figure 1. Stages of chemical processing of GO (a) Pulverized graphite that was used for reduction (b) GO dispersed in water after synthesis using Hummers' method (c) GO thin film.

2.2. X-Ray Diffractometry (XRD)

The X-ray diffraction spectra of graphite powder and GO samples exhibit a sharp peak at $2\theta = 11.2^\circ$ compared to the strong characteristic peak at $2\theta = 26.4^\circ$ for graphite (Figure 2). By using Debye-Scherrer's equation [30], the inter-layer distance for GO sheets was calculated to be 0.82 nm, which is greater than that (0.34 nm) for graphene layers. This increase in the interlayer distance is attributed to the presence of water (H_2O) molecules and various oxygen-containing functional groups as identified by FTIR. This agrees with [36]. These species do facilitate the hydration and exfoliation of the GO sheets. Therefore, the plots in Figure 2 indicate the effectiveness of the modified Hummers' method in oxidizing the graphite leading to increased inter-layer distance between the graphene layers.

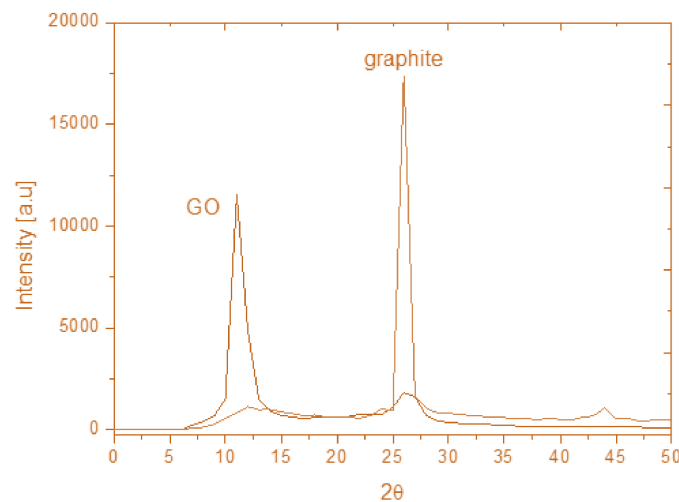


Figure 2. XRD traces for Graphite and GO confirming the synthesis.

It can be observed that the peak at $2\theta = 11.2^\circ$ exhibits higher intensity for the GO material, indicating a higher amount of water molecules/oxygen functional groups present in the basal plane, thus improving the extent of oxidation and reflecting the influence of increased H_2SO_4 in the acidic media. In the case of graphite, this peak is appeared with minor intensity, close to the background of the pattern. The small peaks at $2\theta = 26.4$ degrees for GO sample indicates the presence of unconverted graphite and can be related to the efficiency of the process. The presence of unconverted graphite and the difference in the extent of oxidation were also discerned in the thermal tests in the form of exothermic peaks and varying heat flux for oxidation reactions.

The GO sheets obtained after drying usually exhibit high electrical resistivity but by treating them with hydrohalic acids reducing agents, recovery to an extent is possible. The extent of exfoliation during the reduction of graphite to GO, and the duration of chemical treatment, play a vital role in determining the extent of electrical conductivity restoration. Therefore, an optimum combination of those parameters is paramount to the electrical property restoration.

Investigation of such a complex, multivariable systems and the influence of various parameters on the electrical properties of the reduced GO films individually tend to become tedious, and hence it is difficult to assess the synergistic effects between the parameters. Therefore, partial factorial design of experiments (DoE), accompanied by statistical analysis based on Taguchi method, was used to obtain the best possible combination of these parameters in a minimum number experimental trials.

2.3. Design of Experiments

Three levels of ultrasonication time, reducing agent type and reaction duration were selected (Table 1) to construct an L_9 orthogonal array. Their levels and different combinations are listed in Table 2.

Table 1. Factors for Taguchi L₉ matrix.

Factor	Level 1	Level 2	Level 3
Sonication Time (A)	1 h	10 h	20 h
Reducing Agent (B)	Hydrochloric acid	Hydrobromic Acid	Hydroiodic Acid
Reaction Time (C)	2 h	24 h	48 h

Table 2. Experimental values of electrical resistivity for GO samples.

Standard Order No.	A	B	C	Resistivity (Ω·cm)
1	1	1	1	0.330
2	1	2	2	0.560
3	1	3	3	0.006
4	2	1	2	0.641
5	2	2	3	0.076
6	2	3	1	0.003
7	3	1	3	0.365
8	3	2	1	0.347
9	3	3	2	0.022

The graphical representation of the effect of individual factors and combination of factors towards the overall electrical resistivity is shown in Figure 3. The contribution of each factor towards the overall resistivity is estimated as the average of all the resistivity values when the factor is set at its particular level, thus minimizing any random errors.

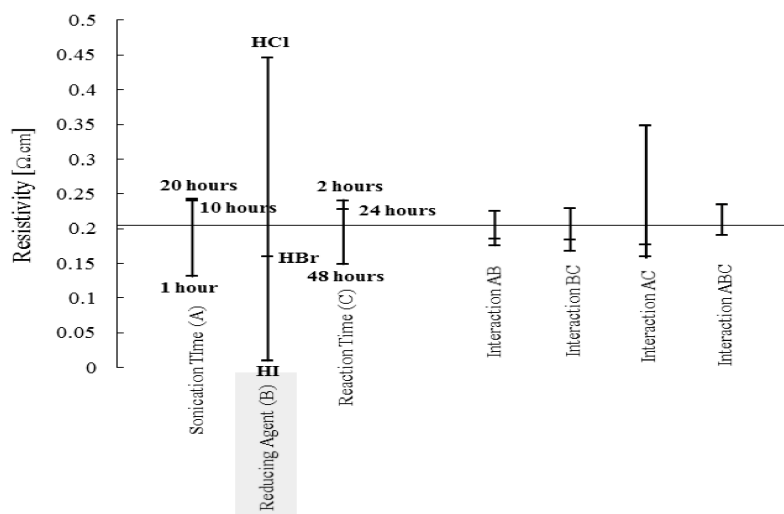


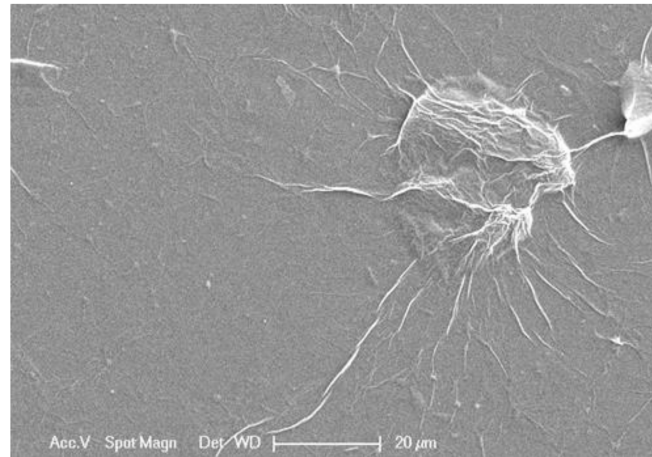
Figure 3. Factor Effect Plot for Taguchi Analysis.

In Figure 3, the overall average of resistivity from all the trials is represented as a horizontal line with the averages of all the individual factors set at their particular levels plotted on either side of it. The physical size of the line determines the factor’s contribution towards the overall response of the system’s electrical resistivity.

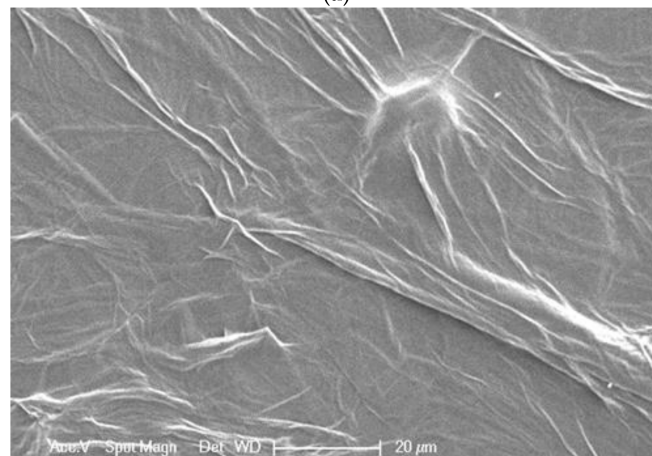
In the factor effects plot the reducing agent type plays a detrimental role in the electrical resistivity (hence increasing the conductivity) of GO. The average resistivity for GO samples treated with hydroiodic acid appear to be in the range of 0.003–0.022 Ω·cm, followed by those treated with hydrobromic acid (0.056–0.347 Ω·cm) and finally with hydrochloric acid (0.33–0.641 Ω·cm).

An increase in ultrasonication time of the GO suspension over 1 h resulted in an increased resistivity, i.e., a decrease in conductivity of the GO. This negative effect for the ultrasonication time

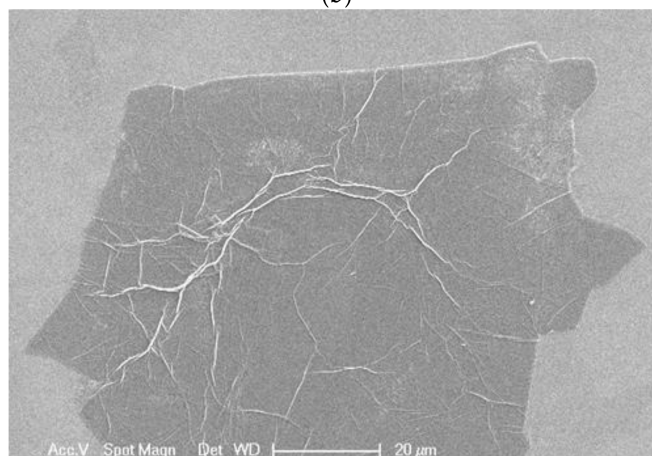
can be attributed to the breaking up of GO sheets into smaller fragments/particulates, rather than an increase in inter-layer distance with increased amount of sonication. The SEM images of GO solutions, subjected to ultrasonication for 1 h, 10 h and 20 h, are presented in Figure 4, respectively, which shows a higher degree of fragmentation of GO sheets with increased ultrasonication.



(a)



(b)



(c)

Figure 4. SEM images of GO after ultrasonication for (a) 1 h that shows relatively less wrinkled sheets (b) 10 h, showing wrinkled features; and (c) 20 h where it is fragmented and wrinkly.

The third factor considered was the reaction time. When the reaction time was increased from 2 h to 48 h, an increase in conductivity was observed. Therefore, an increase in reaction time enhances the overall conductivity of the film. However, the effect is relatively small compared to that of the reducing agent type, because hydroiodic acid produced resistivity as low as 0.003 Ω·cm even at lower reaction times (e.g., at 2 h). Such inferences can be made by evaluating the relevant factor interaction effects, estimated by examining the variation of each factor with respect to their levels.

To understand the synergistic or antagonistic effect of the factors on the overall response of the system, factor interaction plots were used, shown in Figure 5. The size of the lines that are deviating from the average, depict the two factor interaction *sonication time and reaction time* (AC) to contribute more towards the overall conductivity compared to the other factor interactions (*sonication time and reducing agent type* (AB), *reducing agent type and reaction time* (BC) and *sonication time and reducing agent type* (ABC)).

In Figure 5a, the interaction graph for AC displays a drift in the average response values as the ultrasonication time increases from 1 h to 20 h. For the reaction time at its lowest level, i.e., 2 h, the resistivity value drops from 0.33 Ω·cm to 0.003 Ω·cm when the sonication time is changed from 1 h to 10 h, and then it increases to 0.347 Ω·cm with an increase in the sonication time to 20 h. For the reducing time of 24 h, the change in the sonication time from level 1 to 3 (from 1 h to 20 h) results in an antagonistic effect (an increase in resistivity from 0.056 Ω·cm to 0.641 Ω·cm), when the sonication time changes from level 1 to 2, a sudden decrease to 0.022 Ω·cm is observed. For reducing duration of 48 h, the response behavior is similar to that of 2 h with the resistivity value showing an increasing trend, from 0.006 Ω·cm to 0.076 Ω·cm and then to 0.365 Ω·cm, with successive raise in the sonication level.

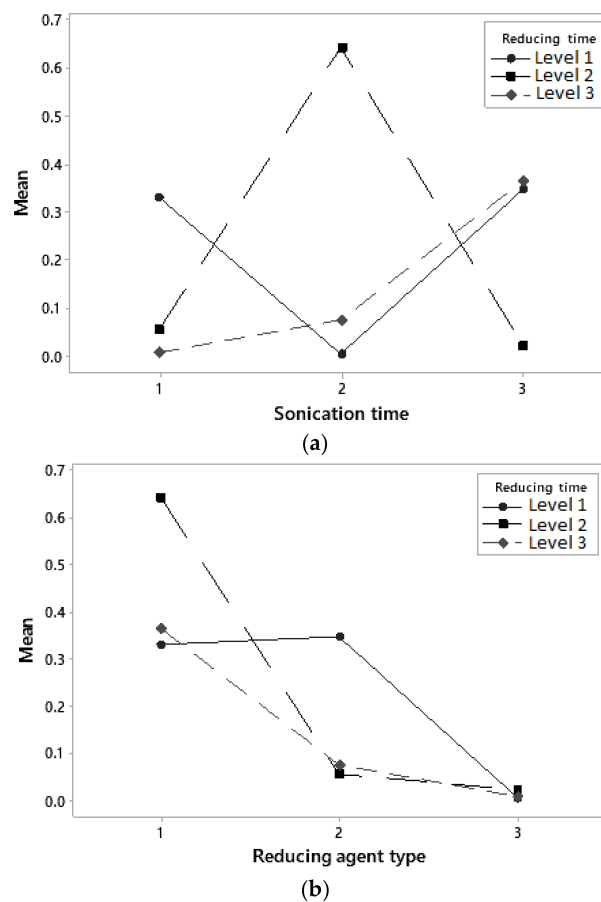


Figure 5. Cont.

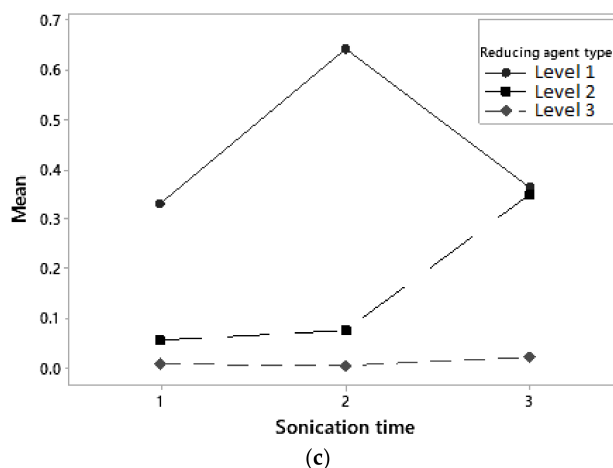


Figure 5. Synergistic and antagonistic interaction effect plots of factors (a) Sonication Time (A) and Reaction Time (C) (b) Reducing Agent (B) and Reaction Time (C) and (c) Sonication Time (A) and Reducing Agent (B).

The interaction graph in Figure 5b shows a change in resistivity with increase in reaction time for each of the reducing agents used (HCl, HBr and HI), with drastic decline in resistivity values observed with HI (from 0.641 $\Omega \cdot \text{cm}$ to 0.056 $\Omega \cdot \text{cm}$). This indicates that the degree of exfoliation is directly proportional to the duration of sonication. For reaction time at its lowest level (2 h), the average resistivity value increases from 0.33 $\Omega \cdot \text{cm}$ to 0.641 $\Omega \cdot \text{cm}$ when the reducing agent is changed from HCl to HI. Therefore, for shorter sonication duration, HCL and HBr provide similar resistivity values and may be preferred over HI. At 48 h sonication, all the reducing agents provide similar exfoliation and hence resistivity values. In Figure 5c, it can be deduced from the antagonistic nature of the interaction effect, the effect of change in the sonication time is most prominent at level 1, but with escalation in the reactivity of the acid used, i.e., at levels 2 and 3 (when using HBr and HI), the effect of sonication becomes less pronounced.

3. Characterization

3.1. Fourier Transfer Infrared Spectroscopy (FTIR)

The spectra obtained by FTIR of graphite and GO samples are shown in Figure 6. A wide band at 3000–3600 cm^{-1} represents the stretching vibration due to the presence of hydroxyl group (O-H vibration). In the spectrum, the typical peaks indicating the oxygen-containing groups are visible as 1715.5 cm^{-1} for C=O (carbonyl/carboxyl), 1337.7 cm^{-1} for carboxylic C-O, 1222.9 cm^{-1} for epoxy C-O and 1060 cm^{-1} for alkoxy C-O. The peak at 1621.5 cm^{-1} corresponding to the in-plane vibrations of aromatic C=C and the skeletal vibrations of the graphene sheets corroborating for the success of oxidation of graphitic domains. The FTIR spectra of GO after treatment with hydrobromic acid (RGO in Figure 6) shows significant decrease of the bands that correspond to C-OH hydroxyl and C=O groups, while the peaks pertaining to epoxy and alkoxy C-O groups have completely disappeared. These FTIR spectra confirm that the GO samples have been significantly de-oxidized and support the hypothesis proposed by Lin et al. [22] that low-temperature reduction processes result in decomposition of carboxylic and carbonyl groups leading to less functional groups in the RGO sample. Though, some residual oxygen-containing species remain in the material.

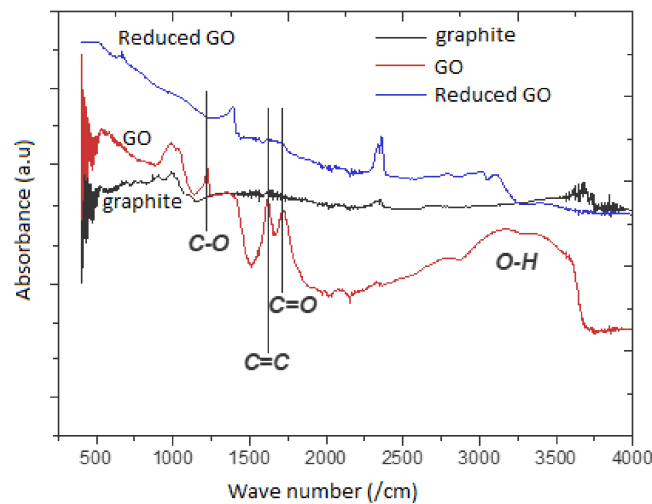


Figure 6. FTIR spectra for Graphite, GO and Reduced GO confirming the reduction process using hydrobromic acid.

3.2. Electromagnetic Shielding

Electromagnetic interference shielding is the attenuation of the incident electromagnetic waves in the material and is expressed by the mathematical formula given by [5,13,31–33].

$$SE = 10 \log \frac{P_i}{P_t} \tag{1}$$

where SE is the shielding effectiveness in decibel (dB), P_t is the power of the transmitted wave and P_i is the power of incident wave. When an electromagnetic wave is incident on a surface, it is absorbed (A), reflected (R) or transmitted (T) and the summation, $A + R + T = 1$ [13] and the attenuation mainly consists of the three components: Absorption A , Reflection R and Multiple Reflections M [32,33]. Hence, the total EMI SE can be expressed as summation of these three components, i.e., $SE = SE_a + SE_r + SE_m$.

The effect of multiple reflections is often negligible when $SE_a \geq 10$ dB [14,32,34,35] as the intensity of an incident wave inside the material after reflection will depend on $(1 - R)$. Therefore, Effective Absorption inside a shielding material is defined using Equation (2) and the SE component rendered by absorption and reflection phenomena can be determined by using Equations (3) and (4) respectively.

$$A_{eff} = \frac{1 - R - T}{1 - R} \tag{2}$$

$$SE_a = 10 \log(1 - A_{eff}) = 10 \log\left(\frac{T}{1 - R}\right) \tag{3}$$

$$SE_r = 10 \log(1 - R) \tag{4}$$

In dynamic fields, the eddy current behaves complexly and it is common practice to develop approximate solutions while modelling shielding enclosures. For thin films, the shielding is dominated by the magnetic field and is governed by the magnetic permeability of the shield. As frequency increases, the shielding mechanism becomes greater due to induced current density that reduces inward from the core, exponentially. The skin depth δ over which the amplitude of incident wave will be effectively reduced is defined by Equation (5) and the SE due to absorption component can be calculated by Equation (6). Therefore, the EMI shielding effectiveness of a composite specimen can be studied as a function of its electrical conductivity which in turn depends on the intrinsic conductivity

of the filler, filler morphology and dispersion and the interfacial interaction between the filler and the matrix molecules [5,12,15,36].

$$\delta = \frac{1}{\sqrt{\pi f \mu \sigma}} \tag{5}$$

where σ is the electrical conductivity in S/cm, μ is the magnetic permeability of the material and is equal to 1 for non-magnetic materials and f is the frequency of incident radiation in MHz.

$$SE_a = K \frac{t}{\delta} = Kt \sqrt{\pi f \mu \sigma} \tag{6}$$

where δ is the skin depth for effective shielding in m , K is the constant for the shield material and t is the thickness of the shield in m .

The thickness of any planar shield can be represented in terms of skin depths to indicate the shielding potential of the material. In addition to the absorption over skin depth, significant reduction of the impinging electromagnetic field can occur through reflection from the shield surface. The formula of far-field reflection loss for a plane-wave radiation is given by Equation (7) [19].

$$SE_r = 108 + \log\left(\frac{\sigma}{f\mu}\right) \tag{7}$$

The maximum value of conductivity attained through chemical reduction of GO sheets was 39,000 S/m. The thickness of the GO films was 0.1 mm and the predicted values of EMI shielding effectiveness for GO thin films are listed in Table 3.

Table 3. EMI SE calculation for reduced GO specimens using hydrobromic acid.

Sr. No.	Electrical Conductivity (S/m)	Frequency (GHz)	EMI Shielding Effectiveness, dB (SE _a)
1	39,000	8	4.13
2	39,000	9	4.38
3	39,000	10	4.62
4	39,000	11	4.84
5	39,000	12	5.06

4. Conclusions

In this paper, GO synthesized from graphite using the modified Hummers’ and Offeman methods was characterized using X-ray diffractometry, Fourier transfer infrared imaging and scanning electron microscopy. The XRD results affirmed the increase in inter-layer distance between graphene layers, and FTIR confirmed the presence of oxygen-containing reactive groups in the oxidized graphite samples. The SEM images revealed typical wrinkled and wavy morphology of GO thin sheets at high magnifications.

A simple, hazard-free, and effective low-temperature chemical reduction method was developed with relatively novel use of hydrohalic acids for removal of oxygen-containing groups from GO. A partial factorial DoE along with Taguchi analysis was used to obtain the best possible combination of parameters, i.e., ultrasonication time, reducing agent and reaction time, to improve the electrical conductivity of reduced GO films. The Taguchi analysis of factorial effects revealed that the effectiveness of the reduction process is primarily dependent on the reducing agent used. Immersion of GO thin films in strong hydrohalic acids, such as hydroiodic acid, can effectively reduce GO even when the reaction time and level of sonication are very low. The post-reduction electrical resistivity values for GO thin films, as measured using the four-point probe method, demonstrated a high degree of improvement in conductivity. The drop in resistivity value after chemical reduction was of the order of 10,000 times, and the measured values were in the range of 0.003–0.641 Ω.cm. The electrical resistivity range obtained in this work is among the lowest reported so far. This suggests the vast

potential of GO-based nanocomposites in applications pertaining to electronic field, where GO could be tuned to exhibit insulating, semiconducting, or conducting behavior, as per the requirement.

Acknowledgments: The authors thank Prateek Jaiswal for assistance with the experimental work and Dong Liu for her assistance with chemical synthesis.

Author Contributions: This work is a part of Jahnavee Upadhyay's ME research at the University of Auckland, and she along with Sanjeev Rao and Raj Das conceived and designed the experiments; Jahnavee Upadhyay under Sanjeev Rao's supervision performed the experiments; Rehan Umer and Kyriaki Polychronopoulou have contributed in analyzing the data; The University of Auckland and Khalifa University of Science and Technology contributed reagents/materials/analysis tools for this work; Sanjeev Rao wrote the paper.

Conflicts of Interest: The authors declare no conflict of interest.

References

1. Kuilla, T.; Bhadra, S.; Yao, D.; Kim, N.H.; Bose, S.; Lee, J.H. Recent Advances in graphene based polymer composites. *Prog. Polym. Sci.* **2010**, *35*, 1350–1375. [[CrossRef](#)]
2. Liang, J.; Wang, Y.; Huang, Y.; Ma, Y.; Liu, Z.; Cai, J.; Zhang, C.; Gao, H.; Chen, Y. Electromagnetic interference shielding of graphene/epoxy composites. *Carbon* **2009**, *47*, 922–925. [[CrossRef](#)]
3. Eda, G.; Unalan, H.E.; Rupensinghe, N.; Amaratunga, G.A.J.; Manish, C. Field Emission from graphene based composite thin films. *Appl. Phys. Lett.* **2008**, *93*, 233502. [[CrossRef](#)]
4. Sengupta, R.; Bhattacharyya, M.; Bandyopadhyay, S.; Bhomicka, A.K. *A Review on the Mechanical and Electrical Properties of Graphite and Modified Graphite Reinforced Polymer Composites*; Elsevier: New York, NY, USA, 2010.
5. Kim, H.; Miura, Y.; Macosko, C.W. Graphene/Polyurethane Nanocomposites for Improved Gas Barrier and Electrical Conductivity. *Chem. Mater.* **2010**, *22*, 3441–3450. [[CrossRef](#)]
6. Compton, O.C.; Kim, S.; Pierre, C.; Torkelson, J.M.; Nguyen, S.T. Crumpled Graphene Nanosheets as Highly Effective Barrier Property Enhancers. *Adv. Mater.* **2010**, *22*, 4759–4763. [[CrossRef](#)] [[PubMed](#)]
7. Choi, W.; Lahiri, I.; Seelaboyina, R.; Kang, Y.S. Synthesis of Graphene and Its Applications: A Review. *Solid State Mater. Sci.* **2010**, *35*, 52–71. [[CrossRef](#)]
8. Yan, J.; Wei, T.; Shao, B.; Fan, Z.; Qian, W.; Zhang, M.; Wei, F. Preparation of a graphene nanosheet/polyaniline composite with high specific capacitance. *Carbon* **2010**, *48*, 487–493. [[CrossRef](#)]
9. Potts, J.R.; Dreyer, D.R.; Bielawski, C.W.; Ruoff, R.S. *Graphene-Based Polymer Nanocomposites*; Elsevier: New York, NY, USA, 2010.
10. Bao, Q.; Zhang, H.; Yang, J.-X.; Wang, S.; Tang, D.Y.; Jose, R.; Ramakrishna, S. Lim, C.T.; Loh, K.P. Graphene-Polymer Nanofiber membrane for ultrafast photonics. *Adv. Funct. Mater.* **2010**, *20*, 782–791. [[CrossRef](#)]
11. Ansari, S.; Giannelis, E.P. Functionalized Graphene Sheet—Poly(vinylidene fluoride) Conductive Nanocomposites. *J. Polym. Sci.* **2009**, *47*, 888–897. [[CrossRef](#)]
12. Stankovich, S.; Dikin, D.A.; Dommett, G.H.B.; Kolhaas, K.M.; Zimney, E.J.; Stach, E.A.; Piner, R.D.; Nguyen, S.T.; Ruoff, R.S. Graphene-based composite materials. *Nature* **2006**, *442*, 282–286. [[CrossRef](#)] [[PubMed](#)]
13. Vovchenko, L.L.; Matzui, L.Y.; Oliynyk, V.V.; Launetz, V.L. The Effect of Filler Morphology and Distribution on Electrical and Shielding Properties of Graphite-Epoxy Composites. *Mol. Cryst. Liq. Cryst.* **2011**, *535*, 179–188. [[CrossRef](#)]
14. Cao, M.-S.; Song, W.-L.; Hou, Z.-L.; Wen, B.; Yuan, J. The effects of temperature and frequency on the dielectric properties, electromagnetic interference shielding and microwave-absorption of short carbon fiber/silica composites. *Carbon* **2010**, *48*, 788–796. [[CrossRef](#)]
15. Yang, Y.L.; Gupta, M.C. Novel carbon nanotube-polystyrene foam composites for electromagnetic interference shielding. *Nano Lett.* **2005**, *5*, 2131–2134. [[CrossRef](#)] [[PubMed](#)]
16. Che, R.C.; Peng, L.M.; Duan, X.F.; Chen, Q.; Liang, X.L. Microwave absorption enhancement and complex permittivity and permeability of Fe encapsulated within carbon nanotubes. *Adv. Mater.* **2004**, *16*, 401–405. [[CrossRef](#)]
17. Park, S.; Ruoff, R.S. Chemical methods for the production of graphenes. *Nat. Nanotechnol.* **2009**, *4*, 217–224. [[CrossRef](#)] [[PubMed](#)]

18. Li, D.; Mueller, M.B.; Gilje, S.; Kaner, R.B.; Wallace, G.G. Processable aqueous dispersions of graphene nanosheets. *Nat. Nanotechnol.* **2008**, *3*, 101–105. [[CrossRef](#)] [[PubMed](#)]
19. Li, D.; Kaner, R.B. Materials science—Graphene-based materials. *Science* **2008**, *320*, 1170–1171. [[CrossRef](#)] [[PubMed](#)]
20. Lerf, A.; He, H.Y.; Forster, M.; Klinowski, J. Structure of graphite oxide revisited. *J. Phys. Chem. B* **1998**, *102*, 4477–4482. [[CrossRef](#)]
21. Yang, Y.; Wang, J.; Zhang, J.; Liu, J.; Yang, X.; Zhao, H. Exfoliated Graphite Oxide Decorated by PDMAEMA Chains and Polymer Particles. *Langmuir* **2009**, *25*, 11808–11814. [[CrossRef](#)] [[PubMed](#)]
22. Lin, Z.; Yao, Y.; Li, Z.; Liu, Y.; Li, Z.; Wong, C.-P. Solvent-Assisted Thermal Reduction of Graphite Oxide. *J. Phys. Chem. C* **2010**, *114*, 14819–14825. [[CrossRef](#)]
23. Saito, H.; Inoue, T. Light and X-Ray Scatterings. In *Polymer Characterisation Techniques and Their Application to Blends*; Simon, G.P., Ed.; Oxford University Press: Washington, DC, USA, 2004; pp. 313–345.
24. Dikin, D.A.; Stankovich, S.; Zimney, E.J.; Piner, R.D.; Dommett, G.H.B.; Evmenenko, G.; Nguyen, S.T.; Ruoff, R.S. Preparation and characterization of graphene oxide paper. *Nature* **2007**, *448*, 457–460. [[CrossRef](#)] [[PubMed](#)]
25. Kang, H.; Kulkarni, A.; Stankovich, S.; Ruoff, R.S.; Baik, S. Restoring electrical conductivity of dielectrophoretically assembled graphite oxide sheets by thermal and chemical reduction techniques. *Carbon* **2009**, *47*, 1520–1525. [[CrossRef](#)]
26. Dreyer, D.R.; Park, S.; Bielawski, C.W.; Ruoff, R.S. The chemistry of Graphene Oxide. *Chem. Soc. Rev.* **2010**, *39*, 228–240. [[CrossRef](#)] [[PubMed](#)]
27. Jang, J.Y.; Kim, M.S.; Jeong, H.M.; Shin, C.M. Graphite oxide/poly(methyl methacrylate) nanocomposites prepared by a novel method utilizing macroazoinitiator. *Compos. Sci. Technol.* **2009**, *69*, 186–191. [[CrossRef](#)]
28. Kilic, A.; Oruc, F.; Demir, A. Effects of polarity on electrospinning process. *Text. Res. J.* **2008**, *78*, 532–539. [[CrossRef](#)]
29. Hummers, W.S.; Offeman, R.E. Preparation of Graphitic Oxide. *J. Am. Chem. Soc.* **1958**, *80*, 1339. [[CrossRef](#)]
30. Cullity, B.D. *Elements of X-Ray Diffraction*; Addison-Wesley Pub. Co.: Reading, MA, USA, 1956.
31. Tesche, F.M.; Ianoz, M.V.; Karlsson, T. *EMC Analysis Methods and Computational Models*; John-Wiley & Sons. Inc.: New Jersey, NJ, USA, 1997.
32. Wang, W.P.; Pan, C.Y. Preparation and characterization of poly(methyl methacrylate)-intercalated graphite oxide/poly(methyl methacrylate) nanocomposite. *Polym. Eng. Sci.* **2004**, *44*, 2335–2339.
33. Pande, S.; Singh, B.P.; Mathur, R.B.; Dhama, T.L.; Saini, P.; Dhawan, S.K. Improved Electromagnetic Interference Shielding Properties of MWCNT-PMMA Composites Using Layered Structures. *Nanoscale Res. Lett.* **2009**, *4*, 327–334. [[CrossRef](#)] [[PubMed](#)]
34. Al-Saleh, M.H.; Sundararaj, U. Electromagnetic interference shielding mechanisms of CNT/polymer composites. *Carbon* **2009**, *47*, 1738–1746. [[CrossRef](#)]
35. Park, K.Y.; Lee, S.E.; Kim, C.G.; Han, J.H. Fabrication and electromagnetic characteristics of electromagnetic wave absorbing sandwich structures. *Compos. Sci. Technol.* **2006**, *66*, 576–584. [[CrossRef](#)]
36. Kim, H.M.; Kim, K.; Lee, C.Y.; Joo, J.; Cho, S.J.; Yoon, H.S.; Pejaković, D.A.; Yoo, J.W.; Epstein, A.J. Electrical conductivity and electromagnetic interference shielding of multiwalled carbon nanotube composites containing Fe catalyst. *Appl. Phys. Lett.* **2004**, *84*, 589–591. [[CrossRef](#)]

